Isı Bilimi ve Tekniği Dergisi, 34, 2, 111-121, 2014
J. of Thermal Science and Technology

ISSN 1300-3615

A CASE STUDY OF COMBUSTION MODELING IN A SPARK IGNITION ENGINE USING COHERENT FLAME MODEL

Ender HEPKAYA*, Salih KARAASLAN, Sıtkı USLU***, Nureddin DINLER** and Nuri YUCEL***

*Tusas Engine Industries Inc., Combustion Aerodynamics Engineer Tepebaşı/Eskişehir Turkey
ender.hepkaya@tei.com.tr
**Department of Mechanical Engineering, Faculty of Engineering, Gazi University
06570 Maltepe Ankara Turkey karaaslansalih@gazi.edu.tr, ndinler@gazi.edu.tr, nuyucel@gazi.edu.tr
***Department of Mechanical Engineering, Faculty of Engineering, TOBB ETU University
06560 Söğütözü Ankara Turkey suslu@etu.edu.tr

(Geliş Tarihi :08.01.2010 Kabul Tarihi: 16.12.2013)

Abstract : In this study, a computer simulation was performed, to visualize fluid flow and combustion characteristics of a single cylinder spark ignition engine. The complete engine cycle process (inlet, compression, expansion and exhaust strokes) in gasoline engine model was investigated using RANS (Reynolds Averaged Navier-Stokes) and CFM (Coherent Flame Model) approaches offered by Star-CD/es-ice. Simulations were done for the compression ratio 8:1 and 1200 rpm engine speed. C_8H_{18} (iso-octane) was used as the engine fuel. In the numerical simulations to model turbulent flow field, k - ε RNG turbulence model was selected with Angelberger wall functions. Static spark advance was set at 20 CA bTDC during the simulations. Fluid flow in the cylinder was observed during all the engine strokes. Especially, just before the exhaust valve open, some numerical abnormal situations were detected. It was observed that the pressure and temperature gradients between cylinder and exhaust port caused these abnormalities at small exhaust valve lifts. Temperature distribution, velocity profiles, burnt-unburnt fuel concentrations were obtained. Courant and Mach numbers were investigated in details at the exhaust stroke. Also global engine parameters such as in cylinder pressure, temperature and heat release rates were plotted. It was observed that CFM combustion model predicts faster flame propagation speed compared to experimental ones. Due to that higher temperature and peak pressure values were obtained in the numerical simulations.
Keywords: CFM combustion model, Star-CD/es-ice, SI engine modeling.

TÜMLEŞİK ALEV MODELİ (CFM) KULLANARAK BUJİ ATEŞLEMELİ BİR MOTORDA YANMA MODELLEME ÇALIŞMASI

Özet : Tek silindirli buji ateşlemeli bir motorda, akış hareketi ve yanma karakteristiğini görselleştirmek amacıyla sayısal bir çalışma gerçekleştirilmiştir. Star CD/es-ice tarafından sağlanan RANS (Reynolds Ortalamalı Navier-Stokes) ve tümleşik alev modeli (Coherent Flame Model - CFM) modelleri kullanılarak benzinli bir motor modelinde tüm motor strokları incelenmiştir. Sıkıştırma oranının 8:1 ve motor hızının 1200 dev/dak. olduğu bir motor simüle edilmiştir. Yakıt olarak C_8H_{18} (n-izooktan) kullanılmıştır. Sayısal simülasyonlarda, türbülanslı akış hareketini modellemek için AngelBelger duvar fonksiyonları ile beraber k-ε RNG türbülans modeli seçilmiştir. Simülasyonlar boyunca statik ateşleme avansı 20 KMA olacak şekilde belirlenmiştir. Tüm stroklarda silindir içi akış hareketi incelenmiştir. Özellikle, egzoz valfinin henüz açtığı zamanda bazı sayısal anormallik içeren durumlar fark edilmiştir. Küçük egzoz valfi açıklıklarında meydana gelen bu anormallikler, silindir ve egzoz portu arasındaki sıcaklık ve basınç farklarından kaynaklanmaktadır. HAD sonuçları kapsamında sıcaklık dağılımı, hız profilleri, yanmış/yanmamış yakıt konsantrasyonları verilmiştir. Egzoz stroğunda elde edilen Courant ve Mach sayıları detaylı bir şekilde incelenmiştir. Ayrıca, silindir içi basınç, sıcaklık ve ısı yayılım oranı gibi glabal motor parametreleri çizilmiştir. Özetle, CFM yanma modelinin kullanıldığı bu çalışmada alev ilerleme hızının beklenen değerlerden yüksek olduğu görülmüştür. Bu nedenle, silindir içinde elde edilen basınç ve sıcaklık değerleri deneysel verilerden daha yüksek olarak elde edilmiştir.
Anahtar Kelimeler: CFM yanma modeli, Star-CD/es-ice, Buji ateşlemeli motor simülasyonu.

INTRODUCTION

CFD models have been extensively validated and used to predict the performance and emissions of spark ignition (SI) and compression ignition (CI) engines. Opposite to the experimental methods, numerical methods are often less expensive and faster. Beside these advantages, simulations give much further

information (mixture formation, combustion process, flow field, etc.) about complex and hard to measure processes in the cylinders. Due to transient, dynamic, turbulent structure and combustion phenomena, it is a complex problem to model an internal combustion engine in-cylinder flow. CFD codes such as STAR-CD, ANSYS Fluent, KIVA etc. are able to solve this kind of problem with their numerical contents and models.

In the literature, numerous studies focused on internal combustion engines and in-cylinder fluid flow and combustion process. Baratta *et al.*(2010) performed a numerical and experimental study about jet formation and fuel-air mixing process in a transparent single-cylinder research engine. The experimental tests were set up at AVL laboratories for double sided PLIF analyses and a finite-volume CFD model was built in STAR-CD/es-ice tool. The numerical model was validated by comparing the ensemble averaged PLIF images to the computed equivalence ratio contours. On the whole, the developed numerical model was able to reasonably reproduce the experimental jet evolution and mixture-formation processes and can be adopted with design and optimization purposes. The combined experimental and numerical analyses allowed a thorough discussion of the mixing characteristics of the engine combustion chamber, both in a stratified and in a homogeneous operating mode. Cho *et al.* (2010) have studied on a four-valve, pent roof, direct-injection spark-ignition (DISI) engine, with the fuel injector located between the two intake valves. They measured and simulated wall film behavior of formation, transport, and vaporization on the surface. To confirm the ability of thermocouples, temperatures were measured to determine the effects of impingement and heat loss associated with fuel film evaporation. The researchers measured high temperature fluctuations during early injection. Simulations of CFD code revealed the evaporation of fuel film was drastically rapid during intake stroke. Therefore, the measured heat loss from the surface could be connected to the heating and evaporation of the fuel film with the wetted area estimated based on CFD results. This is a critical result for predicting the local fuel film thickness from the measured heat loss. The simulations and experiments were in a good agreement for the thickness of fuel film and transport phenomena. As a consequence the researchers validated the spray and impingement models. Choi *et al.* (2002) developed a new model for stratified charged combustion in direct-injection spark-ignition (DISI) engines. In their model they used the secondary diffusion flame in the burned region and the effect of mixture fraction on the laminar burning velocity. Weller's flame area evolution (FAE) model was used and implemented the mixture fraction variation and probability density for primary flame propagation. A two-step reaction mechanism of water-gas shift and hydrogen oxidation was used. They offered a new relationship for the laminar burning velocity. Also, to form a stratified fuel/air mixture, the direct-injection gasoline spray model was mounted into their new model. 3-D simulation was performed for stratified charge combustion in a DISI engine using STAR-CD. The new model simulated flame propagation characteristics, reaction of fuel/air mixture, fractions of products, and temperature. Malaguti and Fontanesi (2009) presented the results of numerical simulation of contemporary gasoline direct injection engine using STAR-CD/es-ice software. They investigated the spray behavior on the walls of combustion chamber. They used the experimentally validated model for spray conditions. So, they concluded choosing the proper models, the injection process and effects of the strategy and location of injection on the wall/fuel interactions could be well demonstrated. Mobasheri and Shahrokhi-Dehkordi (2010) compared three different combustion models, including eddy break-up model (EBU), probability density function (pdf) and coherent flame model (CFM), on a modified 4-cylinder MPFI (Multi Point Fuel Injection) SI engine. They validated the combustion models with the experimental data using appropriate model constants. Also, they concluded the application of EBU model gives the best prediction for the combustion inside the engine cylinder. In another study, CFM-LES and spark ignition models were used (Richard *et al.*, 2007). CFM-LES conforms experimental data and algebraic approaches of other reseacher's. Their results show CFM-LES modeling is independent of flame front resolution.

Koten *et al.* (2010) studied injection effects on the HCCI engine combustion to get nearly full combustion. In other words, nearly zero emissions. They used a model of one cylinder of a six-cylinder diesel engine with nine liters displacement. The comparative results of engine performance depending on compression ratio, injection timing, cone angle and bowl geometry are in good agreement with the results of similar numerical and experimental works. In another numerical study conducted by Koten (2010) is about clean diesel combustion in order to determine low emissions performance. EBU model and Extended Coherent Flame Model (ECFM-3Z) models were used to analyze the combustion and emission formation using Star-CD software in a heavy duty diesel engine. It was concluded that, high turbulence levels influences the low emission formation. Andreassi *et al.* (2009) used a new model for direct injection of gaseous fuels. The offered model, which is based on KIVA-3V, demonstrates the partially stratified charge (PSC) engine operation. D'errico (2008) developed a multi-zone combustion model for the prediction of the performance and exhaust emissions of an engine. Regardless of the limitations of a quasi-dimensional approach, the results are accurate. Application of a reduced chemical scheme was used for the evaluation of NO and CO concentrations, under the different operating conditions with fuels of gasoline and compressed natural gas. Ewald and Peters (2007) developed turbulent burning velocity expression for premixed homogeneous charge spark ignition engine. This expression takes into account the turbulent burning velocity of a planar flame and the influence due to global flame curvature. In spite of a good prediction of

initial flame propagation, there is an under prediction of heat release rate calculation due to swirl. Dinler and Yucel (2010) modeled the combustion in SI engine cylinder. The effects of air/fuel ratio on the combustion were investigated numerically. They offered ignition timing advance with respect engine speed. They used k-ε turbulence modeling and Arrhenius and EBU models in their study. Lecocq *et al.* (2011) modeled abnormal combustion processes in reciprocating engines. They showed that retarding the spark timing delaying the occurrence of knock. In addition to this result, their model had the ability of determining the flame front due to a hot point before spark ignition, which is a factor for knocking.

In this paper, a single cylinder SI engine was analyzed numerically by using STAR-CD/es-ice software. Coherent Flame Model (CFM) was used as combustion model with k-ε-RNG turbulence model. The basic information of the combustion model theory was given in the manuscript content. The flow field, temperature and fuel concentration during combustion were discussed in detail and compared with previous literature studies. Selected cross sections, fuel concentrations and velocity vectors are plotted and interpreted.

NUMERICAL SETUP

The STAR-CD code is based on finite volume method. The code simulates transient, compressible, laminar, turbulent and reacting flows on stationary or moving boundaries, areas and volumes using the equations of the conservation of mass, momentum, energy and species. A modeled 2-valve single-cylinder spark ignition engine was employed for this numerical investigation. In our laboratory, Internal Combustion Engines and Automotive Laboratory of Mechanical Engineering Department of Gazi University, there is a variable compression ratio research engine. The design of the engine studied in this investigation was selected due to this engine. Except valve diameters the remaining dimensions are same. A complete engine cycle including intake and compression strokes, also spark ignition at the end of the compression stroke, expansion and exhaust strokes could be simulated in 3D using the capabilities of the STAR-CD. For modeled engine, a surface model was prepared at the top dead centre (TDC) piston position by using Star CCM+. Top and side views of this surface model are given in Figure 1.

The computational domain was shown in Figure 1. Combustion chamber was modeled with intake/exhaust ports, valves. As seen top views of surface model, two valves are located on the cylinder dome symmetrically. Exhaust and intake valve diameters are chosen 32 mm. Spark plug is located top side of the dome. The specifications and operating conditions of this modeled engine are listed in Table 1.

The computational grid was constructed including the valve and piston motions for a single cylinder spark ignition engine. Star-CD/es-ice module was used to optimize numerical grid structure. Different grid systems were tested in *cold flow and combustion* simulations to decide optimal mesh density. In cylinder pressure were predicted for constant engine speed of 1200 rpm for each case. Element numbers and pressure values of mesh independency analyses were given in Table 2. The theoretical maximum in-cylinder pressure was calculated according to air-standard Otto cycle as 75.12 bar. In the calculations the constants from Pulkrabek (2004), same engine dimensions, and inlet conditions of this study was used.

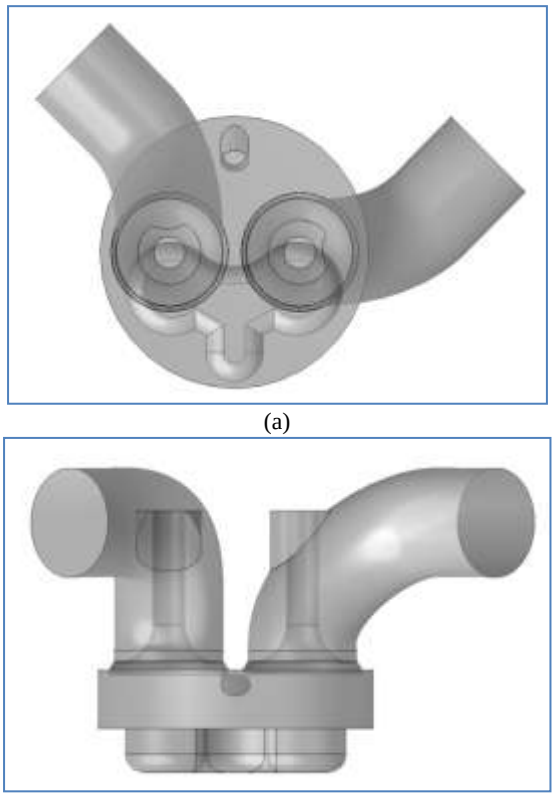

(a)

(b)

Figure 1. (a) Top and (b) side views of surface model.

As seen in this table, by increasing mesh sizes, in-cylinder peak pressure get closer to each other. In the cold flow cases, pressure variations with respect to mesh density were smaller than the combustion cases. In cylinder pressure values for the all mesh density during the crank shaft angle were given in Figure 2.

Table 1. Specifications of the modeled engine.

Bore	76.2 mm
Stroke	111.1 mm
Displacement volume	0.507 lt
Fuel	n-octane/iso-octane
Static spark advance	20° bTDC
Compression ratio	8:1
Intake valve open/close timing	10° bTDC / 36° aBDC
Exhaust valve open/close timing	43° bBDC / 5° aTDC

Table 2. Mesh independency analysis results.

	Combustion (bar)	Cold Flow (bar)
Mesh 1 (152598)	67.01	13.42
Mesh 2 (298672)	69.09	13.58
Mesh 3 (486946)	74.15	13.85
Mesh 4 (693124)	74.39	13.88
Mesh 5 (1025778)	74.47	13.87

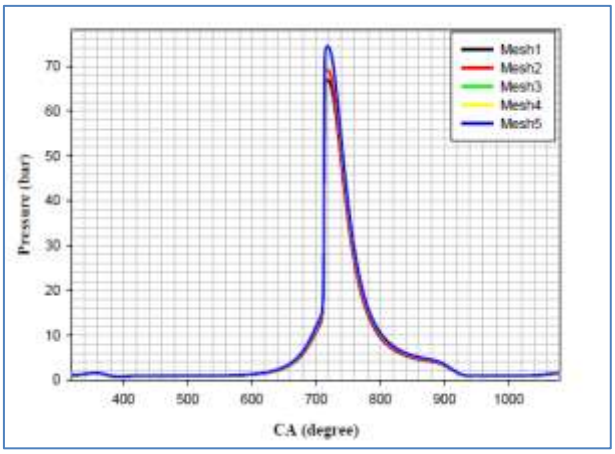

Figure 2. In-cylinder pressure values during the combustion process.

The maximum in-cylinder peak pressure occurs at 715 crank shaft angle for all meshes considered. As expected from these results, the computed solutions show larger deviations for the coarse meshes 1 and 2 while convergence is obtained for finer meshes 3, 4 and 5. Based on the results, grid independence was reached in mesh 3 and therefore, the following simulations have been conducted using this grid. Although both of the medium and fine meshes are under 1% deviation from the finest mesh, medium mesh 4 was chosen to reduce the computation time. The total number of elements for the engine model was chosen 693 124. For all grid structure processes, a 2D template was generated using trimming method. For whole mesh domain, homogeneous 2D template process is an important step. The total amount of elements on 2D template mostly depends on the circumferential cell size. Circumferential cells are used to define the valve features correctly. Also, these cells must be in good agreement with liner and outer rings. Anyway, upper and lower triangular regions were located on 2D template to get compatible grid structure with respect to cylinder liner. In these numerical analyses, hexahedral trimmed cells were created for moving mesh processes. Piston and valve motion were carried out collapsing layers of cells by using es-ice module. Generated 2D template and section of the optimum trimmed numerical grid structure (mesh4) were given in Figure 3.

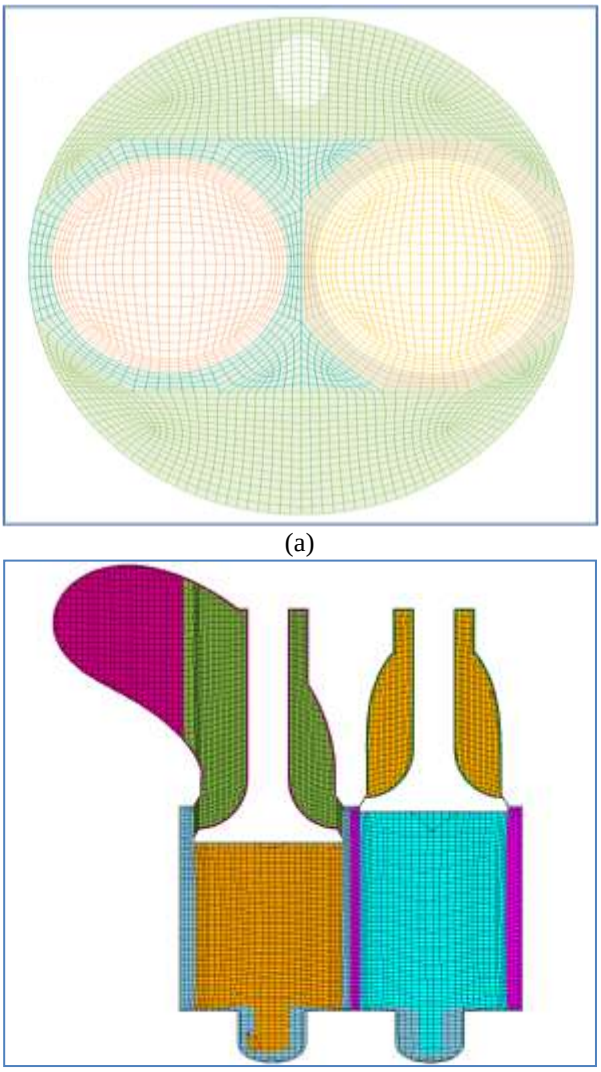

(a)

(b)

Figure 3. View of 2D template and section of trimmed grid structure (a) Top view, (b) side view.

The computational domain includes the intake ports and valves, the cylinder head and piston bowl as shown in Figure 3. Hexahedral cells have used to provide a better accuracy, stability and less computer run time compared to tetrahedral cells. Piston movement and valve lifts were activated by using es-ice module. By the way, the engine geometry was decomposed into moving and stationary parts to reduce interpolating errors. Local mesh densities were introduced in critical regions for exhaust valve narrow gaps between valve seat rings. After trim operation, piston movement and valve lifts were checked. The mesh shown in Figure 2 consists of 693.000 cells, including BDC piston position. The calculation was performed at an engine speed 1200 rpm, compression ratio 8:1, and equivalence ratio of 1. Spark plug ignited at 20^{o} bTDC. The exhaust stroke provided little amount of turbulence in the cylinder and port, thus these effects could be neglected. So, all the simulations started with exhaust stroke (320 CA) and ended 1080 CA. Turbulent fluid flow and combustion characteristics in the engine cylinder were modeled with k-ε RNG and Coherent Flame Model (CFM) respectively. The k-ε RNG model derived by the renormalization group

theory was selected due to its ability to capture highly swirling flows (CD-adapco, 2011b). The model engine was chosen a carbureted fuel supply, so premixed combustion model (CFM) was considered. All the analyses were done at the full load engine operating condition for the constant engine speed of 1200 rpm. The selected properties of CFM model were listed in Table 3.

Table 3. Data used in CFM model.

Combustion Model Properties	**CFM**
α	2.1
β	1
Ignition time, CA	700
Spark plug location (x,y,z), mm	0, 24.506, -5.2926
Ignition delay, s	0.0004
Kernel diameter, mm	1
Mixture fraction	0.06
EGR	disabled
NO_x	disabled
Knock	disabled

The numerical approximation and computation is based on PISO algorithm. Quality cell remediation method was selected in the interface of the software to get a good quality of mesh. This model attempts to identify poor-quality cells based on a set of predefined criteria, such as skewness angle exceeding a certain threshold. Once these cells and their neighbors have been marked, the computed gradients in these cells are modified in such a way as to improve the robustness of the solution (CD-adapco, 2011c). In general, the effect of Cell Quality Remediation is confined to the immediate vicinity of poor-quality and/or degenerate cells, so that the influence on overall solution accuracy is minimal. For the turbulence properties and momentum equations were discretized by using second order upwind differencing method. In an attempt to get more sensitive solution on energy equation, Monotone Advection and Reconstruction Scheme (MARS) differencing method was preferred. The temporal discretization is the implicit method, with variable time step for different engine events. Main time step for the simulations 0.1 CA (1.3×10^{-5} s at 1200 rpm) was chosen (CD-adapco, 2011b). But, it is known that, due to high pressure and velocity gradient especially at exhaust valve early lifts cause some abnormalities (shock region around valve seats). So, time step just before the exhaust valve open was decreased to 0.01 CA. By the way, the Courant number could be stabled. Dynamic effects were not represented due to selection of constant pressure boundary conditions. The walls of the intake and exhaust ports were considered as the fix temperature condition. The valves were assumed as adiabatic wall. The constant temperature boundary conditions were allocated independently for the cylinder head, the cylinder wall, the piston and spark plug that outline the walls of the combustion chamber. Numerical calculations for a complete cycle have last about 56 hours on a 24 CPU-HP z 800 workstation with 24 GB system memory.

Modeling Premixed Turbulent Combustion Based on the CFM

The model's full name is 'Coherent Flame Model with Intermittent Turbulent Net Flame Stretch'. This is a flame area model in which the variable that describes the flame distribution is the flame area density given in Eq. 1 (CD-adapco, 2011a).

$$\Sigma = \overline{\Sigma'} = \lim_{\delta V \to 0} \frac{\overline{\delta A}}{\delta V} \tag{1}$$

where, δA, is the flame area in a volume δV and the overbar denotes ensemble averaging. Transport equation for Σ can be written as

$$\frac{\partial \Sigma}{\partial t} + \nabla.(\langle w \rangle_s \Sigma) = \langle K_T \rangle_s \Sigma + 2\langle K_c S \rangle_s \Sigma$$

where w is the total velocity of the surface, K_T is the flame strain rate, the second term on the right hand side represents flame curvature and $\langle\ \rangle_s$ indicates surface averaging defined as in Eq. 2.

$$\langle\ \emptyset\ \rangle_s = \frac{\overline{\emptyset\Sigma'}}{\overline{\Sigma'}} = \frac{\overline{\emptyset\Sigma'}}{\Sigma} \tag{2}$$

Σ transport equation for a flame surface is modeled as in Eq. 3

$$\frac{\partial \Sigma}{\partial t} + \nabla.(u\Sigma) - \nabla.\Gamma_\varepsilon \Sigma = \alpha K_t \Sigma - \beta \frac{\rho_u Y_{ft} S_u (1 + \frac{a\sqrt{k}}{S_u})}{\bar{\rho}\, Y_f} \Sigma^2 \tag{3}$$

where K_t is the net flame stretch, ρ is the gas density, k is the turbulence kinetic energy, S is the unstrained laminar flame speed, α , β and a are the model coefficients and subscript u denotes the unburnt gas. The first term on the right hand side of this equation represents the flame area increase due to the combined effects of strain rate and curvature and the second term represents the flame area decrease due to fuel consumption. Note that the latter term significantly destroys the flame surface only when the fuel mass fraction Y_f goes to zero, i.e. when all the fuel is consumed (CD-adapco, 2011a).

The net flame stretch is calculated from the Intermittent Turbulent Net Flame Stretch (ITNFS). This model uses experimental data about intermittent turbulence to determine the distribution of stretch along the flame front and direct numerical simulations of flame-vortex interactions to construct a library of the net flame stretch function K_t. To simplify the use of their results for engineering calculations, they curve-fitted their library data in the form of a dimensionless net flame stretch function involving the following parameters

$$\Gamma_K = \frac{K_t}{\varepsilon/k} = f(\frac{u'}{S_u}, \frac{I_l}{\delta_l}) \tag{4}$$

Here ε is the turbulence dissipation rate, u′ is the turbulence intensity, I_l is the integral length scale defined as

$$I_l = \frac{c_\mu^{3/4}}{\kappa} * \frac{k^{3/2}}{\varepsilon} \quad (5)$$

where c_μ and κ are the turbulent viscosity coefficient and von Karman constant of the k-ε model, respectively, and finally δ_l is the thermal laminar flame thickness calculated following as

$$\delta_l = 2\frac{\mu_b}{Pr\rho_u S_u} \quad (6)$$

In this expression, Pr is the laminar Prandtl number of the burnt gas, assumed to be constant and equal to 0.9 and μ_b is the molecular viscosity of the burnt gas calculated from Sutherland's law

$$\mu_b = \frac{\mu_1 T_b^{1.5}}{\mu_2 + T_b} \quad (7)$$

where μ_1 and μ_2 are coefficients

$\mu_1 = 1.457x10^{-6}$ $kgm^{-2}K^{-1.5}$

$\mu_2 = 110$ K

and T_b is the burnt gas temperature. The mean reaction rate used in the transport equation for the regress variable b is

$$\omega_{cfm} = -\rho_u S_u \Sigma \quad (8)$$

Ignition treatment for the CFM-ITNFS model

The ignition treatment for the CFM-ITNFS model in STAR is a simplified version of the approach proposed by Boudier *et al*. (1992). In the original approach, the ignition period is treated in two distinct phases. In the first phase, an electric discharge occurs between the electrodes and heats up the mixture to ignition point. An approximately spherical kernel forms with a rapidly expanding reaction zone. The propagation speed increases from its minimum value and asymptotically approaches the laminar flame speed for a planar unstretched flame, given by (CD-adapco, 2011a)

$$S_{u\infty} = \frac{T_b}{T_u} S_u \quad (9)$$

The assumed spherical kernel growth during this stage can be calculated from an ordinary differential equation

$$\frac{dr}{dt} = \frac{T_b}{T_u} S_u \quad (10)$$

When the kernel propagation speed reaches the value of $S_{u\infty}$, the first transition criterion is met. This is denoted as the first transition time t_1; the kernel at this time has reached the radius r_1.

During the second stage, it is assumed that the reaction zone of the laminar kernel still propagates with the laminar flame speed, augmented by the expansion ratio, but is simultaneously wrinkled and thickened by turbulence. The kernel radius is still calculated from equation but the kernel surface area during this phase equals the sum of the area of the spherical laminar kernel and the area of the wrinkles. The rate of increase of the kernel area is calculated from

$$\frac{dA}{dt} = \frac{d}{dt}\left(4\pi r^2(t)\right) + (\alpha K_t A) \quad (11)$$

The first term on the right-hand side of this equation represents the increase of the kernel surface due to laminar propagation. The second term is the rate of the area increase due to the turbulent stretch, given by equation. The initial conditions for these two equations are

$r(t_1)=r_1$

$A(t_1)=4\pi r_1$

The second stage ends when the second transition criterion is met. This is defined as the time t_2 when the laminar stretch K_l,

$$K_l = \frac{1}{A_l}\frac{dA_l}{dt} = \frac{2}{r}\frac{dr}{dt} \quad (12)$$

It is assumed that the ignition kernel does not influence the in-cylinder flow and temperature fields during these processes. Ultimately, it is the second transition time t_2 and the kernel area at that time that are used for the initialization of the turbulent premixed combustion model. The last operation of the ignition treatment is the initialization of the flame-area per- unit-volume variable Σ. It is assumed that at $t = t_2$, the Σ distribution is a double error function (CD-adapco, 2011a).

$$\Sigma(r, t_2) = \frac{A_2}{\Omega_\infty}\left\{1 - \mathrm{erf}\left(\frac{|r - r_2|}{2l_2}\right)\right\} \quad (13)$$

where Ω_∞ is the normalisation volume

$$\Omega_\infty = \int_0^\infty 4\pi u^2 \left\{1 - \mathrm{erf}\left(\frac{|u - r_2|}{2l_2}\right)\right\} du \quad (14)$$

which ensures that at time t2 on an infinite domain

$$A_2 = \int_0^\infty 4\pi u^2 \, \Sigma(u, t_2) du \quad (15)$$

The quantity l_2 is the diffusion length scale at time t_2 defined as

$$l_2(t) = \sqrt{\frac{\nu_t}{\sigma_\Sigma}(t_2 - t_1)} \quad (16)$$

where ν_t is the kinematic viscosity and σ_Σ is the Schmidt number for Σ.

RESULTS

After the simulations were completed, the primary results were examined firstly. These results contain in-cylinder pressure, temperature and engine indicator diagram as seen in Figure 4. After the time of ignition (700 CA) and with 0.0004 s delay, pressure and temperature values increase slightly. The volume averaged peak pressure and the peak temperature during the cycle are about 74.4 bar and 3120 K, respectively.

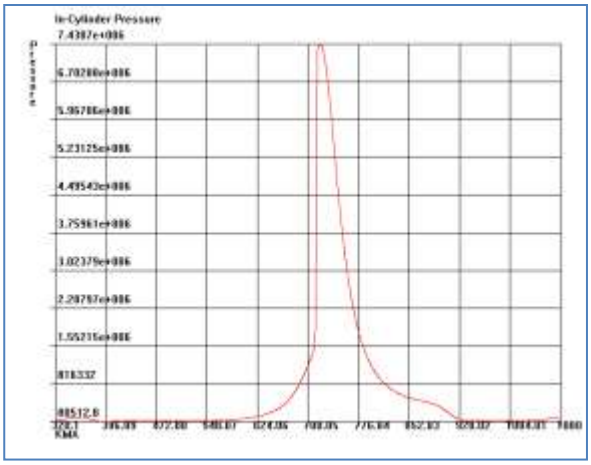

(a)

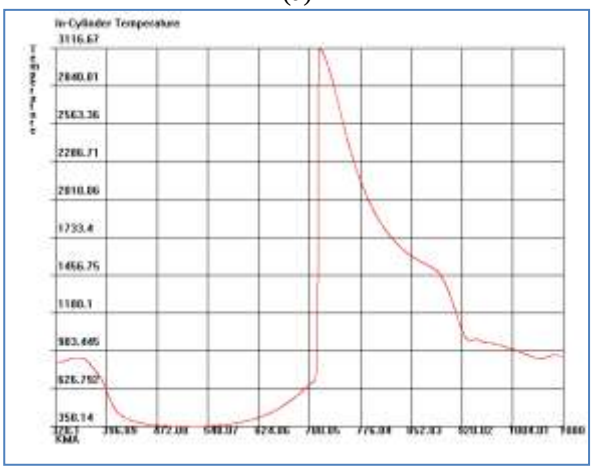

(b)

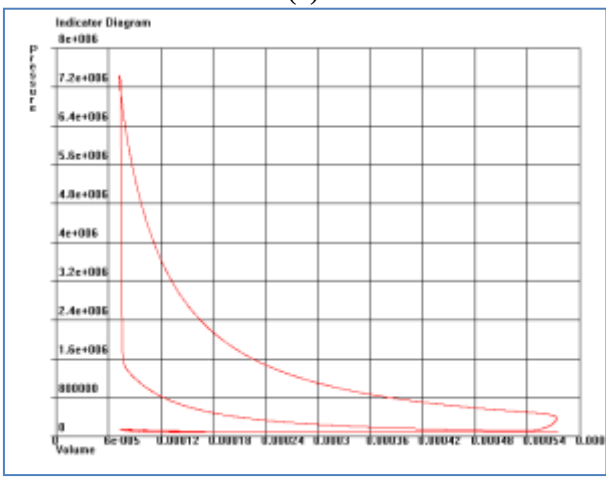

(c)

Figure 4. In-cylinder (a) pressure, (b)temperature and (c) engine indicator diagram graphs.

With the expansion and exhaust strokes, these values decreased to normal exhaust conditions (0.8 bar and 880 K). Those peak values are higher than the experimental data obtained from similar engine combustion chamber model. The flame speed of the homogenous charge for stoichiometric fuel/air ratio is faster than the lean or rich equivalence ratio cases.

The secondary results (contours, vectors etc.) were examined on a section plane B-B which was shown in Figure 5. This section plane was located at symmetry section of spark plug to visualize burnt-unburnt regions with their temperatures and the gas mixture velocities during combustion.

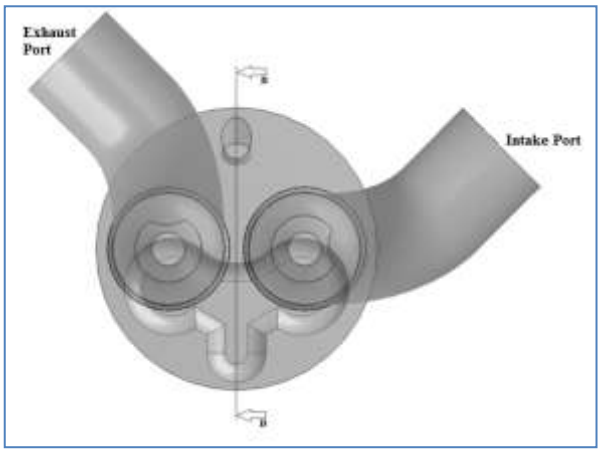

Figure 5. Spark plug region section plane.

In Figure 6, the fuel concentration contours of 702, 706, 710 and 712 CA, were visualized on the spark plug section plane. It can be seen that there is not any change in fuel concentration at 702 CA due to 0.0004 s ignition delay. This delay corresponds to 2.88 CA; therefore, combustion starts at 702.88 CA (Figure 5 (b)). At 706 CA, the fuel concentration decreased to zero inside the core and the flame front propagates up to cylinder walls in 25-30 CA. At the beginning of the combustion flame propagates spherically, then due to high turbulence in the cylinder and the geometry of the combustion chamber the shape of the flame front deformed. In Figure 6 (c) and (d) concentration variation was seen clearly. Behind the flame front, fuel concentration was decreased to zero. The velocity vectors near TDC were given in Figure 6. After the ignition, the stationary gas mixture has started to move from spark plug to the bowl structure due to high pressure and heat release. When the piston came close to TDC, cylinder pressure increase and the piston bowl started to behave tumble generator. It is seen Figure 7(b), the 706 CA piston position, there were tumble motion on the piston bowl. It is known that tumble motion served the mixing process in the cylinder. This squish motion can be seen more effectively near TDC and maximum magnitude of the velocity vectors raised up to 70-75 m/s (Figure 7(d)). High speed inside the cylinder causes to increase in turbulence intensity, which results fast reaction rates.

Temperature distribution of burnt gas for two different section planes (side view, top view) during combustion period in the cylinder were given in Figure 8. If the temperature contours were compared with the fuel concentration variations given in Figure 6, it can be seen that there are in consistent. The static spark ignition

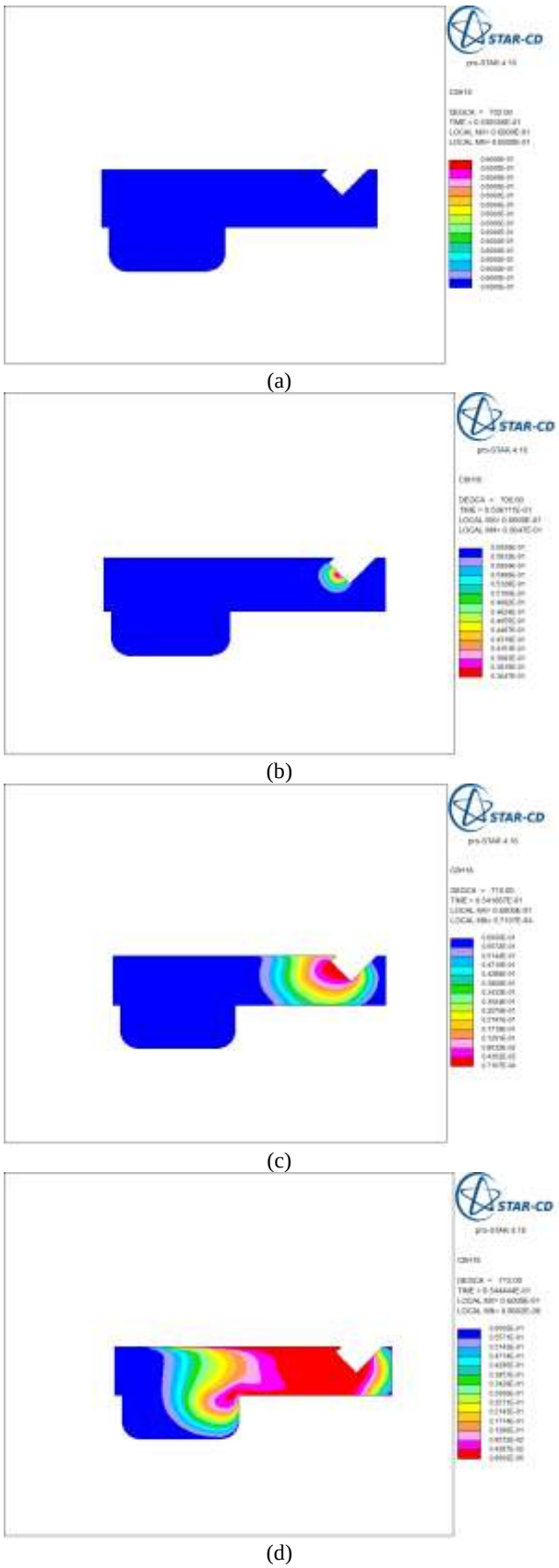

(a)

(b)

(c)

(d)

Figure 6. Fuel concentration variation during combustion process at (a) 702 CA, (b) 706 CA, (c) 710 CA, (d) 712 CA.

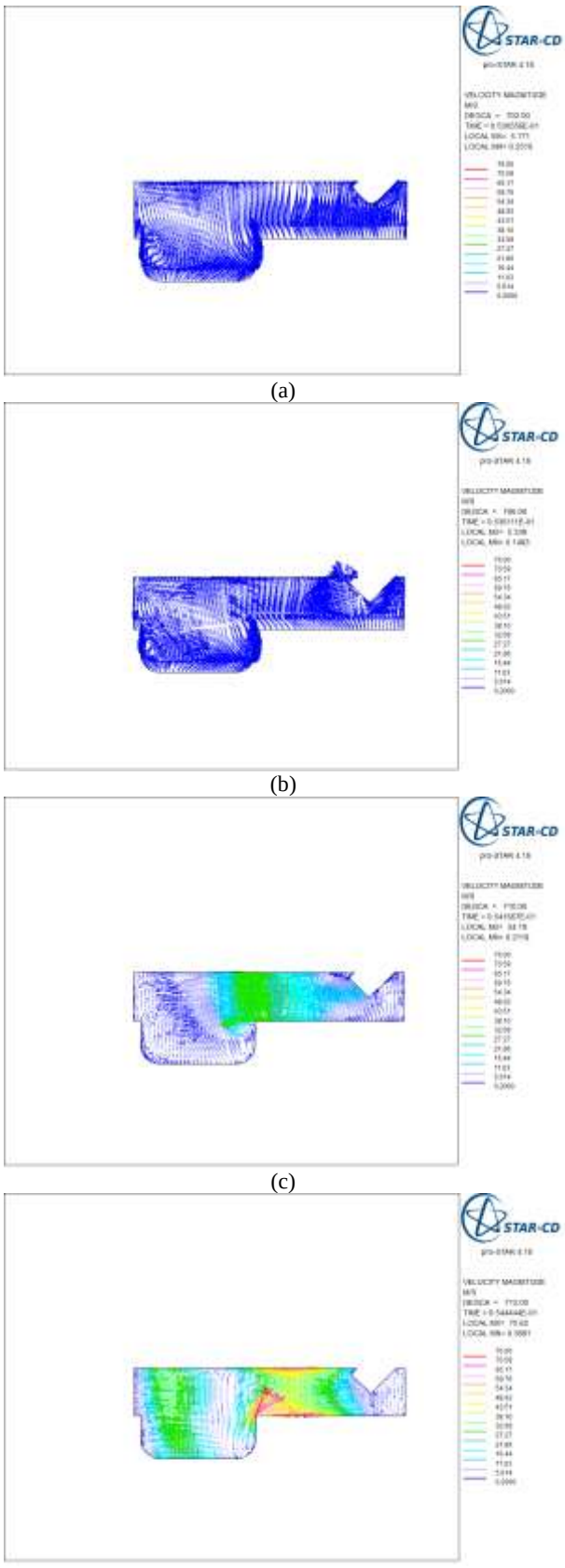

(a)

(b)

(c)

(d)

Figure 7. Velocity vectors of inside the cylinder at (a) 702 CA, (b) 706 CA, (c) 710 CA, (d) 712 CA.

advance was 20 CA bTDC (700 CA position for the solution) piston position. As seen in Figure8, flame propagation has not started at 702 CA, yet, due to ignition delay period. The temperature values up to 702 CA show that compression heating effect of air-fuel mixing process. At 702 CA, there was a temperature distribution between 607 and 670 K due to compression heating process and after ignition, the temperature of the gas mixture has increased suddenly. When the specific heat ratio was chosen 1.37 ($k=C_p/C_v$) for the air standard cycle. Peak temperature would occur at the end of the compression stroke TDC piston position. The calculated theoretical peak temperature is 632 K. So, the numerical temperature value of air-fuel mixture at the end of the compression stroke is in the acceptable range.

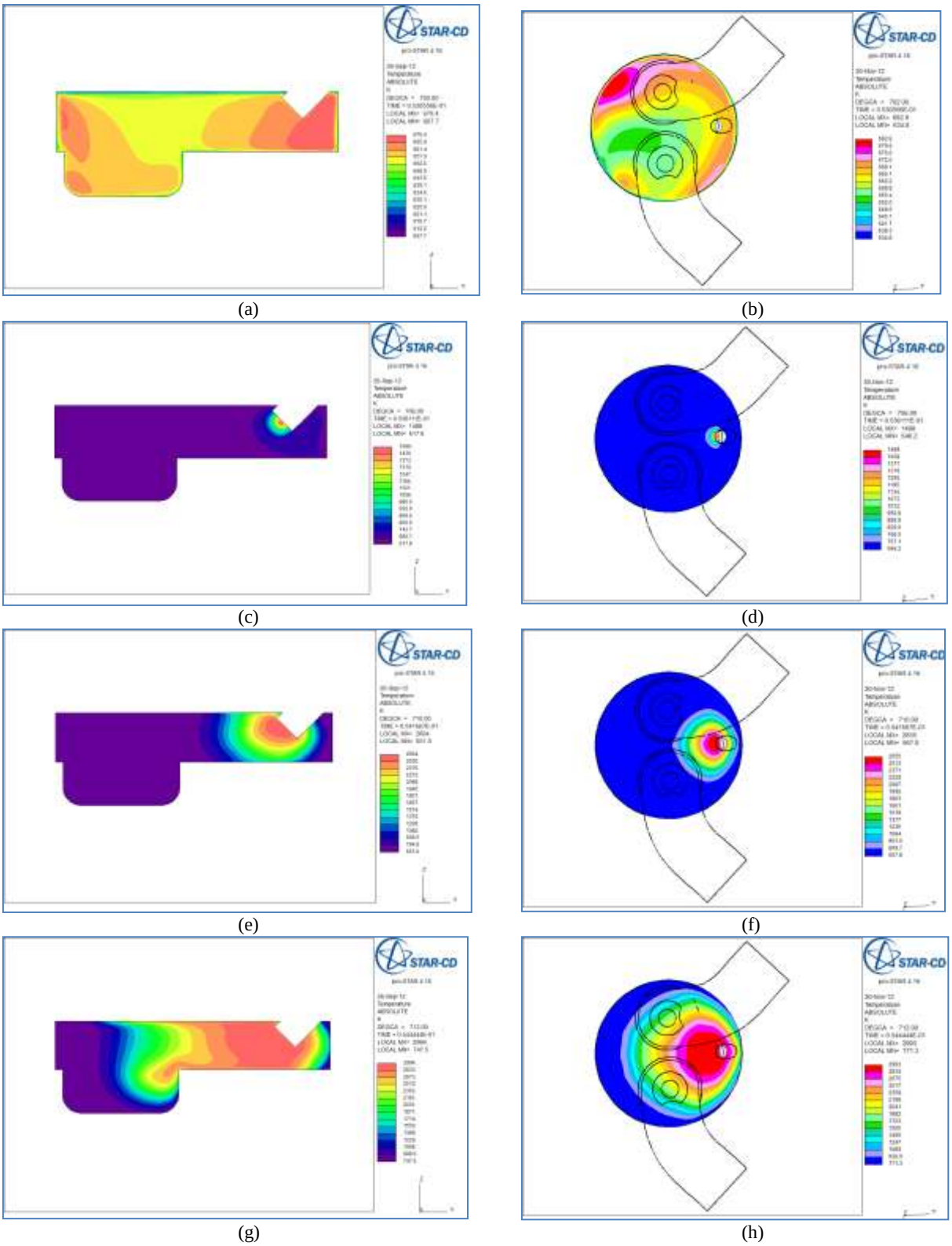

Figure 8. Temperature contours of gas mixture during combustion process at (a),(b) 702 CA, (c),(d) 706 CA, (e),(f) 710 CA, (g),(h) 712 CA.

We know that spark plug ignited at 700 CA, and combustion started at 702.88 CA due to 0.0004 s ignition delay. It is seen that, the temperature reached to 1490 K at the centre of spark plug just after ignition timing (706 CA) (Figure 8 (c)-(d)) and the flame started to surge. While the piston was moving to TDC, the core temperature of the spark plug increased continuously. When the flame reached the center of the cylinder, the core temperature was about 2650 K. At the 712 CA (Figure 8 (g)-(h)), it is seen that 80% of the combustion process has been completed. Combustion process was completed in 25-30 CA. Hot gas mixture (about 3150 K) have almost filled cylinder entirely. Then, expansion and exhaust strokes have been started and the cycle has completed. In this numerical study, peak value of cylinder pressure reached to 74 bar just after the TDC piston position. Exhaust valve opens 43 CA bBDC for this engine model. When the exhaust valve started to open, the initial gap was 0.1 mm between valve and valve stem. At this piston position, there were high temperature and pressure gradient occurred between cylinder and exhaust port. These results caused high Mach and Courant numbers at this stage of cycles. To handle this abnormal conditions, time step size was decreased and pressure correction relaxation factor was taken 0.3. These numerical approaches made analyzes more stable and accurate.

One of the major operating variables that affect spark-ignition engine performance, efficiency and emissions at any given load and speed is spark timing. Effect of 3 static spark timing BTDC on cylinder pressure was also investigated in this study. Cylinder pressure values for different spark advance was shown in Figure 9.

Figure 9 shows the effect of spark advance variations on wide open throttle cylinder pressure at selected engine speed. If combustion starts too early in the cycle, the work transfer from the piston to the gases in the cylinder at the end of the compression stroke is too large; if combustion starts too late, the peak cylinder pressure is reduced and the expansion stroke work transfer from the gas to the piston decreases. If the end of the combustion process is progressively delayed by retarding the spark timing, the peak pressure occurs later in the expansion stroke and is reduced in magnitude. These changes reduce the expansion stroke work transfer from the cylinder gases to the piston. As seen from figure maximum cylinder pressure occurs at 30^{o} spark advance BTDC. As the spark timing advancing, in-cylinder pressure increases as expected. However, it does not mean that the maximum in-cylinder pressure obtained at the optimum spark timing value. When the CFD simulation results are examined for 1200 rpm, MBT (maximum brake torque) is obtained at 20 CA bTDC (before top dead center). The optimum timing which gives the maximum brake torque occurs when the magnitudes of these two opposing trends just offset each other.

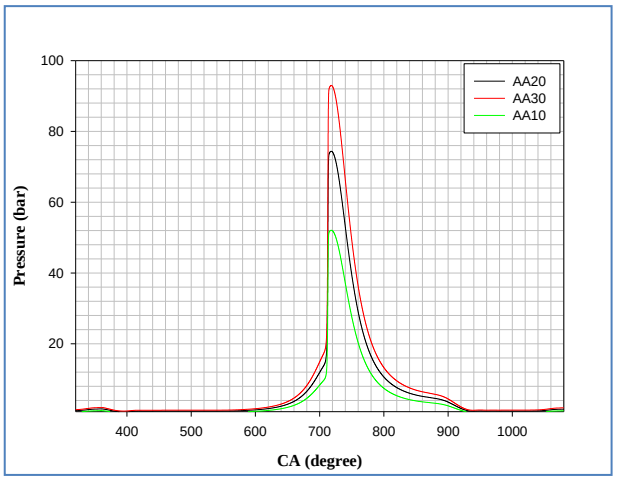

Figure 9. In cylinder pressure for different static spark advance operating conditions.

In premixed combustion, the fuel-oxidizer mixture flammability limit lies between the equivalence ratios 0.5 to 1.5 approximately (Peters, 2000). In the present study, the numerical simulation flammability limits were examined and it was determined between 0.72 and 1.28 for these simulations performed under operating conditions. Out of these values, the ignition and flame propagation have failed and pressure and temperature distribution were almost same as the cols flow results.

CONCLUSION

In this numerical study, three dimensional CFD simulations were performed for a single cylinder internal combustion engine. The grid structure and mesh motion events were set up in STAR-CD/es-ice and flow and combustion processes were solved by STAR solver. The Coherent Flame Model (CFM) was used as combustion model and k-ε-RNG model was used as turbulence model. In results, the pressure, temperature and fuel concentration after spark ignition were investigated and interpreted in details.

The peak pressure and temperatures were higher than experimental values and the combustion process was observed very fast, it has ended in 25-30 CA. The flame speed that effected the combustion duration, was slowed up by the turbulent flame speed coefficient, by this way, the combustion process last 50-60 CA. When the exhaust valve started to open, it was seen that some abnormal velocity and temperature values around the exhaust valve due to high gradients. These problems were solved by using small time steps and low relaxation factors.

When the results of CFM combustion model are analyzed, in-cylinder pressure, temperature and indicator diagram are obtained as expected trends. Nonetheless, when the stroke and bore dimensions of the model engine are taken into account, obtained values of peak pressure, and temperature values are over the expected values. Fuel concentrations at various cross-sections reveal the structure of flame behavior

looks like a diffusion flame propagation like diesel combustion. Flame propagates faster than expected and this causes shorter combustion duration. After the ignition of spark plug, the spherical flame front is expected, however, it is seen that there is a different distribution. After the ignition of spark plug, the flame front is not spherical as expected. The analyses of flow and combustion characteristics inside the engine cylinder exhibit the acceptable trends. Still, for more consistent results G-equation and ECFM-32 spark ignition and combustion models could be used to compare the results of CFM.

ACKNOWLEDGMENT

The authors would like to acknowledge Scientific Technological Research Council of Turkey (TUBİTAK). This study was supported by the Scientific Technological Research Council of Turkey under Grant of Support Programme for Scientific and Technological Research Project (Project Code: 109M420).

REFERENCES

Andreassi L., Facci A.L., Ubertini S., 2009, A Multidimensional Model to Simulate Direct Gaseous Fuel Injection in Internal Combustion Engines, *Proceedings of the ASME Internal Combustion Engine Division 2009 Spring Technical Conference (ICES2009)*, Milwaukee, Wisconsin, USA, 477-486.

Baratta M., Catania A.E., Pesce F.C., 2010, Computational and Experimental Analysis of Direct CNG Injection and Mixture Formation in a Spark Ignition Research Engine, *Proceedings of the ASME 2010 Internal Combustion Engine Division Fall Technical Conference (ICEF2010)*, San Antonio, Texas, USA, 777-793.

Boudier, P., Henriot, S., Poinsot, T., Baritaud, T. 1992. A Model for Turbulent Flame Ignition and Propagation in Spark Ignition Engines, *24th Symp. (Int.) on Combustion, The Combustion Institute*, 503-510.

Cho K., Grover R. O., Assanis D., Filipi Z., Szekely G., Najt P., Rask R., 2010, Combining Instantaneous Temperature Measurements and CFD for Analysis of Fuel Impingement on the DISI Engine Piston Top, *J. Eng. Gas Turbines Power*, 132, 7.

Choi H., Kim M., Min K., Lee J., 2002, The Stratified Combustion Model of Direct-Injection Spark-Ignition Engines, *Proceedings of the Combustion Institute*, 29, 1, 695–701.

CD-Adapco, 2011a, STAR Methodology for Internal Combustion Engine Applications.

CD-Adapco, 2011b, Best Practices Guide for I.C. Engines.

CD-Adapco, 2011c, es-ice User Guide.

D'Errico G., 2008, Prediction of the Combustion Process and Emission Formation of a Bi-fuel SI Engine, *Energy Conversion and Management*, 49, 11, 3116–3128.

Dinler N., Yucel N., 2010, Combustion Simulation in a Spark Ignition Engine Cylinder: Effects of Air-Fuel Ratio on the Combustion Duration, *Thermal Science*, 14, 4, 1001-1012.

Ewald J., Peters N., 2007, On Unsteady Premixed Turbulent Burning Velocity Prediction in Internal Combustion Engines, *Proceedings of the Combustion Institute*, 31, 2, 3051–3058.

Koten H., 2010, Comparison of Various Combustion Models within a Multidimensional Framework Applied To Heavy Duty CI Engine, *Proceedings of ICFD 10: Tenth International Congress of Fluid Dynamics*, Egypt.

Koten H., Yılmaz M., Gül M.Z., 2010, Numerical study on a heavy duty CI engine to achieve ultra-low emissions, *Proceedings of the ASME 2010 Internal Combustion Engine Division Fall Technical Conference (ICEF2010)*, San Antonio, Texas, USA, 319-328.

Lecocq G., Richard S., Michel J.B., Vervisch L., 2011, A new LES model coupling flame surface density and tabulated kinetics approaches to investigate knock and pre-ignition in piston engines, *Proceedings of the Combustion Institute*, 33, 2, 3105–3114.

Malaguti S., Fontanesi S., 2009, CFD Investigation of Fuel Film Formation within a GDI Engine under Cold Start Cranking Operation, *Proceedings of the ASME Internal Combustion Engine Division 2009 Spring Technical Conference (ICES2009)*, Milwaukee, Wisconsin, USA, 555-562.

Mobasheri R., Shahrokhi-Dehkordi M. S. S., 2010, A Comparative Study of Combustion Models for Spark Ignition Engines Based on Experimentation and CFD Simulation, *Proceedings of the ASME 2010 Internal Combustion Engine Division Fall Technical Conference (ICEF2010)*, San Antonio, Texas, USA, 289-299.

Peters N., 2000, Turbulent Combustion, Cambridge Monograhs on Mechanics, Cambridge University Press.

Pulkrabek W.W., 2004, *Engineering Fundamentals of the Internal Combustion Engine* (2nd Edition), Pearson Prentice Hall, ABD.

Richard S., Colin O., Vermorel O., Benkenida A., Angelberger C., Veynante D., 2007, Towards Large Eddy Simulation of Combustion in Spark Ignition Engines, *Proceedings of the Combustion Institute*, 31, 9, 3059–3066.